

Diyne-Containing PPVs: Solid-State Properties and Comparison of Their Photophysical and Electrochemical Properties with Those of Their Yne-Containing Counterparts

Daniel Ayuk Mbi Egbe,^{*,†} Benjamin Carbonnier,[‡] Elisabeth Lekha Paul,[§] David Mühlbacher,[⊥] Thomas Kietzke,[§] Eckhard Birckner,[#] Dieter Neher,[§] Ulrich-Walter Grummt,[#] and Tadeusz Pakula[‡]

Institut für Organische Chemie und Makromolekulare Chemie der Friedrich-Schiller Universität Jena, Humboldtstr. 10, D-07743 Jena, Germany; Max-Planck-Institut für Polymerforschung, Ackermannweg 10, D-55128 Mainz, Germany; Institute of Physics, University of Potsdam, Am Neuen Palais 10, D-14469 Potsdam, Germany; Konarka Austria Forschungs-u. EntwicklungsGmbH, Gruberstr. 40-42, A-4010 Linz, Austria; and Institut für Physikalische Chemie der Friedrich-Schiller-Universität Jena, Lessingstr. 10, D-07743 Jena, Germany

Received April 11, 2005; Revised Manuscript Received May 23, 2005

ABSTRACT: Diyne-containing poly(*p*-phenylene–vinylene)s, **4a–d**, of general chemical structure $-(\text{Ph}-\text{C}\equiv\text{C}-\text{C}\equiv\text{C}-\text{Ph}-\text{CH}=\text{CH}-\text{Ph}-\text{CH}=\text{CH}-)_n$, obtained through polycondensation reactions of 1,4-bis(4-formyl-2,5-dioctyloxyphenyl)-buta-1,3-diyne (**2**) with various 2,5-dialkoxy-*p*-xylylenebis(diethylphosphonates), **3a–d**, are the subject of this report. The polymers exhibit great disparity in their degree of polymerization, *n*, which might be ascribed to side-chain-related differences in reactivity of the reactive species during the polycondensation process and which led to *n*-dependent absorption (solution and solid state) and emission (solution) behaviors of the polymers. Polarizing optical microscopy and differential scanning calorimetry are employed to probe their thermal behavior. The structure is investigated by means of wide-angle X-ray diffraction for both isotropic and macroscopically oriented samples. Comparison of photophysical (experimental and theoretical) and electrochemical properties of the polymers with those of their yne-containing counterparts **6a–d** $[-(\text{Ph}-\text{C}\equiv\text{C}-\text{Ph}-\text{CH}=\text{CH}-\text{Ph}-\text{CH}=\text{CH}-)_n]$ has been carried out. Similar photophysical behavior was observed for both types of polymers despite the difference in backbone conjugation pattern. The introduction of a second yne unit in **4** lowers the HOMO and LUMO levels, thereby enhancing the electron affinity of polymers **4** compared to polymers **6**. The “wider opening” introduced by the second yne unit facilitates moreover the movement of charges during the electrochemical processes leading to minimal discrepancy, ΔE_g , between the optical and electrochemical band gap energies. Polymers **6**, in contrast, show significant side-chain-dependent ΔE_g values. Low turn-on voltages between 2 and 3 V and maximal luminous efficiencies between 0.32 and 1.25 cd/A were obtained from LED devices of configuration ITO/PEDOT:PSS/polymer **4**/Ca/Al.

Introduction

Semiconducting polymers have recently attracted considerable attention from both fundamental and practical points of view.¹ The electronic and optical properties of such compounds are synthetically tunable through structural modifications. The grafting of adequate solubilizing agents enable their processability into transparent films, a precondition for their use as advanced materials in various domains of applications, such as light-emitting diodes,^{2–4} field effect transistors,^{5–7} and photovoltaic devices.^{8–10}

Among conjugated polymers, poly(phenylene–vinylene)s (PPVs) have been most widely studied, especially since the first report of electroluminescence by the group in Cambridge in 1990.² The focus on PPVs was furthermore upheaved after the discovery of ultrafast photoinduced femtosecond charge transfer from alkoxy-substituted PPV to the Buckminsterfullerene by Saric-

iftci and Heeger in 1992.¹¹ A great number of PPV derivatives have been designed to suit various specific areas of applications.¹ Polymers containing diyne group in the main chain¹² have been basically designed for nonlinear optical investigations, resulting from the fact that such compounds exhibit very high second- and/or third-order nonlinear optical susceptibility.^{13–15} In this contribution we focus on diyne-containing PPVs of the following general constitutional unit: $-(\text{Ph}-\text{C}\equiv\text{C}-\text{C}\equiv\text{C}-\text{Ph}-\text{CH}=\text{CH}-\text{Ph}-\text{CH}=\text{CH}-)_n-$, **4a–d**. This was purposely done to compare their properties with those of their yne-containing congeners: $-(\text{Ph}-\text{C}\equiv\text{C}-\text{Ph}-\text{CH}=\text{CH}-\text{Ph}-\text{CH}=\text{CH}-)_n-$ bearing identical alkoxy side chains, **6a–d**.¹⁶ This is in line with our previous studies on hybrid phenylene–ethynylene-*alt*-phenylene–vinylene polymers. Such polymers exhibit enhanced electron affinity and higher photoluminescence efficiencies than PPV.^{17–20} The question to be answered here is, what effect does the replacement of yne units through diyne units have on photophysical (absorption, emission, fluorescence kinetics) and electrochemical properties of these PPV derivatives? Theoretical calculations have been taken into considerations to substantiate the experimental findings. Solid-state characterization of the synthesized polymers was performed by means of various experimental techniques, and the results are discussed with respect to the molecular characteristics.

[†] Institut für Organische Chemie und Makromolekulare Chemie der Friedrich-Schiller Universität Jena.

[‡] Max-Planck-Institut für Polymerforschung.

[§] University of Potsdam.

[⊥] Konarka Austria Forschungs-u. EntwicklungsGmbH.

[#] Institut für Physikalische Chemie der Friedrich-Schiller-Universität Jena.

* Corresponding author: Tel (+49)-(0)-3641-948267; Fax (+49)-(0)-3641-948202; e-mail c5ayda@uni-jena.de.

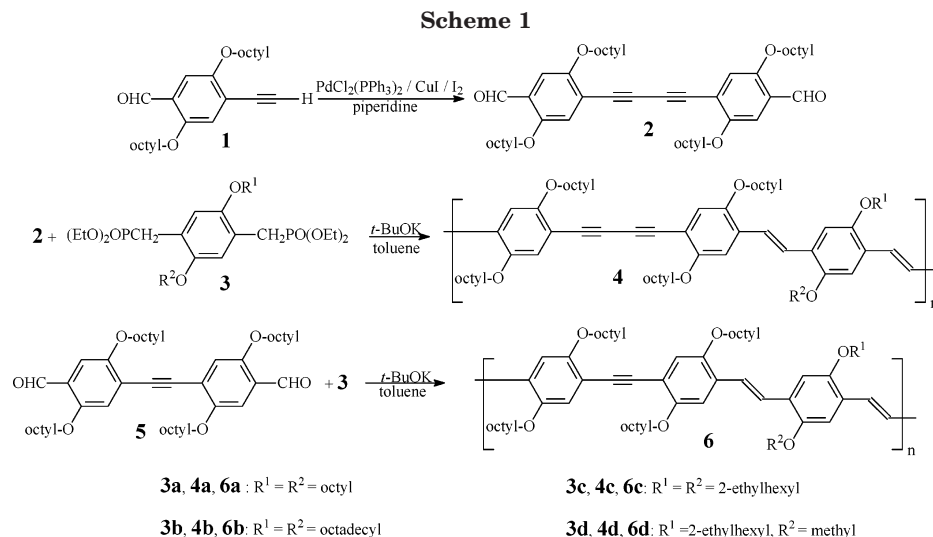


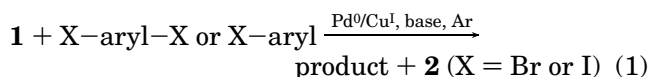
Table 1. Molecular and Thermal Characteristics for the Synthesized Diyne-Containing PPVs

code	\bar{M}_n^a	\bar{M}_w^a	\bar{M}_z^a	M_p^a	PDI ^a	n^a	$T_{5\%}^b$ [K]
4a	8600	19000	35900	12900	2.20	8	631
4b	5200	11900	24900	4900	2.28	4	614
4c	24000	70500	130000	70000	2.93	22	629
4d	4100	8500	15 700	3300	2.07	4	628

^a Data from GPC obtained using THF as eluent and polystyrene as standard. ^b Temperature at which 5% weight loss was recorded during the thermogravimetric analysis.

Results and Discussion

Synthesis and Characterization. The synthetic path to polymers **4a–d** is illustrated in Scheme 1. The compounds were obtained through the Horner–Wadsworth–Emmons olefination reaction of various dialkoxy-substituted bisphosphonate esters **3** with diyne-containing dialdehyde **2**. Dialdehyde **2** is always obtained as a byproduct in 2–7% yield during the Sonogashira Pd-catalyzed cross-coupling reaction²¹ of 1-ethynyl-4-formyl-2,5-dioctoxybenzene (**1**)¹⁷ with aryl halogenide or aryl dihalogenide, as shown in eq 1.^{16,18b,19b}



The direct conversion of **1** into **2** is achieved in yields around 80% through the jointly Pd- and Cu-catalyzed oxidative coupling in the presence of iodine and piperidine (Scheme 1). Polymers **4a–d** were obtained as orange-red materials in yields between 72 and 87% after reaction times between 2 and 3.5 h. They are soluble in common organic solvents such as chloroform, THF, dichloromethane, toluene, and chlorobenzene. Data from GPC (THF and polystyrene as standard) are given in Table 1. All the polymers are characterized with a polydispersity index around 2. However, there are considerable discrepancies between the degrees of polymerization, n , in total contrast to polymers **6a–d**, where n values around 7 were obtained for all the polymers.¹⁶ This might suggest differences in reactivity depending on the side chains grafted on the bisphosphonate esters. An attempt, for example, to increase the n value of **4b** by prolonging the reaction time to 6 h brought no significant changes.

The chemical structure of the polymers was confirmed through ¹H and ¹³C NMR, IR, and elemental analysis.

The ¹³C NMR spectrum of **4c** in deuterated chloroform is depicted in Supporting Information Figure S1. The various signals could be readily assigned to their corresponding carbons, except the signal of the triple bond carbons, which however was detected in the infrared spectroscopy around 2140 cm⁻¹ as a weak peak.

Thermal Behavior. Thermal behavior of the four diyne-containing PPVs was evaluated by means of TGA, POM, and DSC. All polymers exhibited remarkable thermal stability, and the lowest temperature for 5% weight loss was 614 K for **4b** (Table 1). Polymers **4** are birefringent as observed after polymerization and melt into isotropic liquid with increasing temperature. The major differences were noticed upon cooling from the isotropic states. For **4a**, **4b**, and **4c** birefringent textures were observed to develop (for an example see Supporting Information Figure S2), while **4d** retained its black appearance even below room temperature. On the basis of these microscopic observations, the high-temperature endotherms seen in the DSC traces are assigned to the isotropization of the polymers (Figure 1). The complex thermal behavior of the polymers can be recognized from the data presented in Figure 1, where especially the polymers' endothermic transitions, as observed during the first and second heating runs, differ considerably. Despite their rather complex melting, reorganization ability of **4a** and **4c** is evidenced by unique exothermic peak. The transitions observed for **4b** in the low-temperature range are presumed to reflect the order–disorder transitions of the longer octadecyloxy side chains. The DSC analysis indicates that polymer **4d** is partially amorphous after fast cooling (10 K min⁻¹) from isotropic melt confirming the POM observations. No changes in the microscopic textures were observed for any of the transition preceding the isotropization. This finding suggests that the macromolecular arrangements are nearly the same for all the phases.

Structural Ordering. Powder samples were initially examined both at room temperature and in isotropic phase (Supporting Information, Figure S3). The data collected at room temperature indicate correlations over large distances for the four samples and over short distances for the octadecyloxy-substituted polymer **4b**. The position of the low-angle diffraction peaks seems to be correlated with the molecular structure since the related periodicities increase accordingly with the length of the side chains. For measurements performed in the

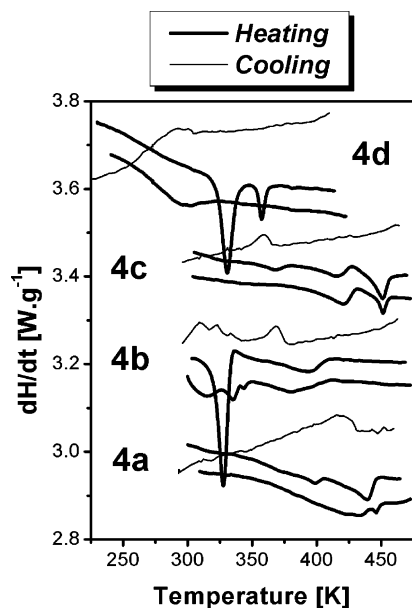


Figure 1. DSC thermograms recorded for the bulk diyne-containing (PPV)s during heating (thick lines) and cooling (thin lines) with the rate 10 K min^{-1} . Both first (upper traces) and second heating (lower traces) runs are presented for each polymer.

isotropic phases, the low-angle intensity maxima reveal that the long-distance correlations are partially preserved and the diffuse wide-angle halos reflect the disordered molecular arrangement. The structure of diyne-containing PPVs was further examined for extruded filaments. The mechanical deformation involved alignment of chains along the fiber axis and in general has led to an improved order on the molecular scale. For the uniaxial orientation, long-range correlations were detected along the equatorial and in some cases along the meridional directions (Figure 2). The equatorial reflections are assigned to the transversal periodicities between polymer backbone-related structures such as layers. The meridional scattering indicated additional ordering in the direction parallel to the orientation of the macromolecular chains. The periods extracted from the position of the meridional reflections for **4a** and **4c** assumed a value of about 2.2 nm, nearly matching the chemical repeating unit length in fully extended conformation (Chem 3D Ultra 7.0). Such translationally correlated arrangement of the polymer chains was not detected for polymers **4b** and **4d** having the lowest degree of polymerization ($n = 4$) of the series. For **4b**, the wide-angle scattering exhibited intensity maximum along the meridional direction and indicated a distance of 0.42 nm. These findings suggest that long octadecyloxy side groups may provide strong cohesive forces influencing the packing in the solid state. For the other polymers, we presumed that the wide-angle intensity maxima detected along the equatorial direction reflect mainly the interchain distances within self-ordered assemblies.

Effect of temperature on the organized structures has been examined for **4a**, **4b**, and **4c** samples in the oriented state. In the temperature ranges correlating well with the transitions detected by means of DSC, changes were also noticed in the 2D WAXS patterns. Herein, we will limit our discussion to the changes observed for **4a** and **4c** during heating to temperatures below the isotropic phases. With the temperature increase, the long-range equatorial correlations remained

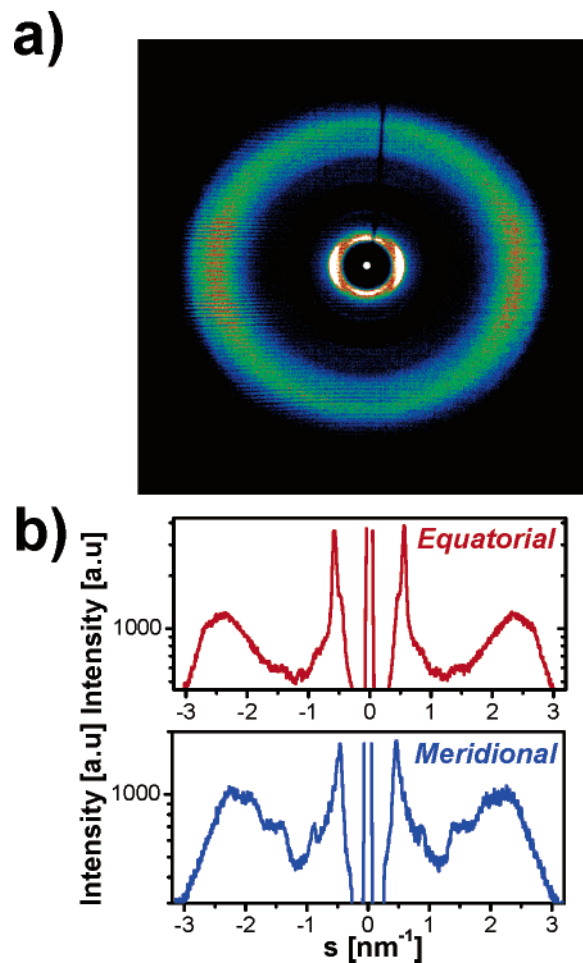


Figure 2. (a) 2D X-ray diffraction pattern recorded for macroscopically oriented filament of **4c**. (b) Intensity distributions measured along the equatorial (horizontal) and meridional (vertical) directions in the 2D pattern.

nearly the same, but the meridional reflections lost gradually their intensity and diffuse halos appeared at wide angles. These scattering effects indicate that within the high-temperature supramolecular organization the chains are translationally uncorrelated. The changes observed were perfectly reversible, and initial ordering was recovered after slow cooling to room temperature.

Photophysical Investigations. The photophysical properties of the polymers were investigated in dilute chloroform solution as well as in solid state. The optical data are summarized in Table 2, namely the absorption peak maxima, λ_a , the extinction coefficients at the peak maxima, ϵ_{max} , the optical band gap energy, E_g^{opt} (calculated from $\lambda_{10\% \text{ max}}$, wavelength at which the extinction has dropped to 10% of the peak value),^{18b} the emission maxima, λ_e , the Stokes shift, the full width at half-maximum of the absorption and emission spectra, fwhm_a , fwhm_e , and the fluorescence quantum yields, Φ_f . The emission spectra were obtained after exciting at λ_a . Table 3 summarizes data from the fluorescence kinetics measurements, namely fluorescence lifetime, τ , fluorescence rate constant, k_f , the rate constant of radiationless deactivation, k_{nr} , the fluorescence rate constant according to Strickler and Berg, $k_f(\text{SB})$, and the ratio between k_f and $k_f(\text{SB})$. Figure 3 depicts the dilute solution absorption and emission spectra of polymers **4a–d** as well as **6a–d**. The photophysical data ($\lambda_a \sim 470 \text{ nm}$, $\lambda_e \sim 525 \text{ nm}$, $\Phi_f \sim 70\%$, and $\tau \sim 0.7 \text{ ns}$) as well as the

Table 2. Data from Absorption and Emission Spectra in Dilute Chloroform Solution (10^{-5} – 10^{-6} M) and in Solid Thin Films of the Polymers

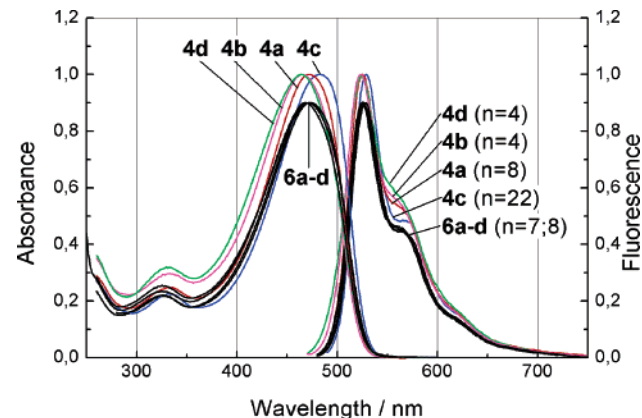
code	λ_a [nm]	ϵ_{\max}^c [$M^{-1} \text{ cm}^{-1}$]	fwhm_a [cm^{-1}]	E_g^{opt} [eV]	λ_a^d [nm]	Stokes shift ^e [nm (cm^{-1})]	fwhm_e [cm^{-1}]	Φ_f^f [%]
4a^a	473	71 700	4100	2.36	525	52 (2100)	2100	67
4a^b	493		4800	2.17	553, 592	60 (2200)	2700	21
4b^a	465	53 000	4700	2.35	524	59 (2400)	2200	67
4b^b	478		5500	2.19	552, 594	74 (2800)	2200	32
4c^a	483	91 000	4000	2.33	529	46 (1800)	1500	68
4c^b	520		4400	2.19	552, 592	32 (1100)	2100	23
4d^a	464	58 800	5000	2.36	523	59 (2400)	2300	71
4d^b	478		5700	2.21	551	73 (2800)	2400	44
6a^a	468	60 300	4500 ^g	2.36	524	56 (2300)	1900	70
6a^b	491		5000	2.17	556, 593	65 (2400)	2300	19

^a Solution. ^b Solid state. ^c Per mole of the repeating unit in the case of the polymers. ^d Italic data indicate the major peak. ^e $\lambda_e - \lambda_a$ ($1/\lambda_a - 1/\lambda_e$). ^f Fluorescence quantum yield, $\pm 10\%$. ^g The fwhm_a values in solution for **6b**, **6c**, and **6d** are respectively 4300, 4600, and 4300 cm^{-1} .

Table 3. Fluorescence Lifetimes in CHCl_3 Solution and Rate Constants of the Deactivation Processes

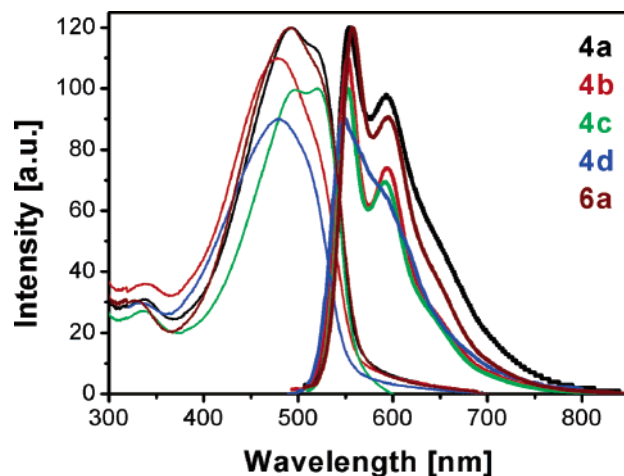
code	τ_f^a ns	k_f^b ns ⁻¹	$k_f(\text{SB})^c$ ns ⁻¹	$k_f/k_f(\text{SB})$	k_{nr}^d ns ⁻¹
4a	0.73	0.92	0.54	1.7	0.45
4b	0.77	0.87	0.43	2.0	0.43
4c	0.66	1.03	0.66	1.6	0.48
4d	0.76	0.93	0.50	1.9	0.38
6a	0.77	0.91	0.48	1.9	0.39
6b	0.76	1.03	0.53	2.0	0.29
6c	0.71	1.01	0.52	1.9	0.39
6d	0.74	0.86	0.41	2.1	0.49

^a Fluorescence lifetime, ± 0.05 ns. ^b Fluorescence rate constant: $k_f = \Phi_f/\tau$. ^c Fluorescence rate constant according Strickler and Berg: $k_f(\text{SB}) = 2.88 \times 10^{-9} \times n^2 \times \int F(\nu)/\nu^3 d\nu / \int F(\nu) d\nu \times \int \epsilon(\nu)/\nu d\nu$, where $\epsilon(\nu)$ = absorption coefficient, for the polymers per repeating unit, n = refractive index of the solvent, and $F(\nu)$ = corrected fluorescence spectrum. ^d Rate constant of radiationless deactivation: $k_{\text{nr}} = (1 - \Phi_f)/\tau$.

**Figure 3.** Normalized absorption and emission spectra of polymers **4a–d** and **6a–d** in dilute chloroform solution.

spectra show that there are no significant differences in both types of compounds. The almost twice smaller fwhm_e (relative to fwhm_a) and the more structured fluorescence spectra are indications of enhanced rigidity and planarization in the singlet excited state, S_1 . From the ratio $k_f/k_f(\text{SB})$, it can be concluded that the effective chromophore consists of 1.5–2 repeating units in diyne- and yne-containing polymers; i.e., the diyne units do not interrupt the conjugation despite the small rotational energy barrier between the phenylene units. However, a closer look at the absorption maxima as well as the shape of the absorption and emission spectra shows a small but significant increase of the band position with increasing degree of polymerization (Figure 3).²²

This is ascribed to the higher probability of finding longer effective conjugated segments (higher coplanarity

**Figure 4.** Normalized thin film absorption and emission spectra of polymers **4a–d** and **6a**.

of phenylene units) with increasing polymer chain length in the S_0 state. The more pronounced shoulder in the fluorescence spectra with increasing chain length is due to the restricted amplitude of bending motions of the excited chromophore in longer polymer chains.

The solid-state absorption and emission spectra are depicted in Figure 4. Similar to the solution, there is a correlation between the degree of polymerization, n , and the solid-state absorption maximum, λ_a , whereby a gradual red shift of λ_a is observed with increasing n . For example, both **4b** and **4d** with $n = 4$ absorb at $\lambda_a = 478$ nm and exhibit almost similar fwhm_a value around 5500 cm^{-1} despite the differences in side chains. Whereas polymers **4a** and **6a**, both having $n = 8$, but different conjugation patterns, show similar absorption behavior ($\lambda_a \sim 490$ nm, $\text{fwhm}_a \sim 5000 \text{ cm}^{-1}$), which moreover proves that replacing yne through diyne leads to no changes in the photophysical behavior of the polymers. Polymer **4c**, with $n = 22$, has the longest wavelength maximum at $\lambda_a = 520$ nm.

The emission spectra of all the polymers except **4d** are well structured and consist of two maxima around 552 and 592 nm. In the case of **4d**, the emission spectrum clearly shows only the peak around 551 nm; the peak around 592 nm appears as a discrete shoulder. In general, the shape and the relative intensity of both emission maxima as well as the fwhm_e values depend more on the nature of the side chains attached at R^1 and/or R^2 than on the degree of polymerization n . However, polymers **4b** and **4d**, with lowest n values of 4, show higher solid-state fluorescence quantum yields of 32 and 44%, respectively, probably due to less

Table 4. Comparison of Electrochemical Data of 4a–d and 6a–d with MDMO-PPV^{25 a}

code	$E_{\text{peak}}^{\text{OX}}$ [mV]	$E_{\text{peak}}^{\text{RED}}$ [mV]	$E_{\text{onset}}^{\text{OX}}$ [mV]	$E_{\text{onset}}^{\text{RED}}$ [mV]	HOMO [eV]	LUMO [eV]	E_{g}^{ec} [eV]	ΔE_{g} [eV]
4a	+1125		+710	−1570	−5.46	−3.18	2.28	0.11
4b	+1215		+760	−1590	−5.51	−3.16	2.35	0.16
4c			+760	−1590	−5.51	−3.16	2.35	0.16
4d	+1095		+710	−1560	−5.46	−3.19	2.25	0.04
6a	~+1000	−2010	+565	−1725	−5.32	−3.03	2.29	0.12
6b		~−1980	+665	−1765	−5.42	−2.99	2.43	0.25
6c		~−2000	+740	−1695	−5.49	−3.06	2.45	0.22
6d	+885	−1930	+645	−1725	−5.4	−3.03	2.37	0.18
PPV	+670		+510	−1750	−5.26	−3	2.26	0.14

^a All potential values are shown vs NHE; NHE level used for HOMO–LUMO calculation was -4.75 eV.^{26,27}

radiationless deactivation pathways. Polymers with higher n values (4a, 4c, and 6a) exhibit Φ_{f} values around 20%.

Theoretical Considerations. Density functional theory implemented in the Gaussian03 package²³ was used to optimize the geometry of both types of polymers. The model chemistry used was b3lyp/6-31g(d). Although alkoxy side chains enhance conjugation due to their electron-donating property, the calculations were first done only with unsubstituted polymers in order to reduce the calculation effort because we frequently encountered convergence problems.

After successful geometry optimization using periodic boundary conditions and the default convergence criteria, the difference densities between the S_1 and S_0 were calculated for the repetition unit and a series of oligomers comprising up to five repetition units (rhf/6-31g(d)). Hydrogen atoms were attached to the chain terminals. The results were visualized with the help of the GAUSS-VIEW program. It is obvious from Supporting Information Figures S4 and S5 that the regions of electron redistribution on the chain remain nearly unchanged upon increasing the number of repetition units from 4 to 5. Thorough inspection reveals that the diyne-containing polymer converges a little faster than the yne-containing one. However, in addition to the intrinsic limitation of the conjugation length obtained for the idealized coplanar chain geometry, there is another limitation introduced at finite temperature by the conformational flexibility of the polymer chain. We have recently calculated the torsional barrier for tolane as 3.4 kJ/mol.²⁴ With the same model chemistry (b3lyp/6-31+g(d)), we find 0.85 kJ/mol for 1,4-diphenyldiethynyl. Transition state optimization resulted in a barrier of 0.92 kJ/mol. The rotational barrier of 2,5,2',5'-tetrahydroxytolane was calculated as 6.2 kJ/mol (6.0 kJ/mol for the transition state). We neither could optimize a 90° twisted structure nor were able to localize a transition state due to convergence problems with the model compound 2,5,2',5'-diphenylbutadiyne using the (b3lyp/6-31+g(d) model chemistry.

To get an upper limit of the rotational barrier, we simply performed single-point calculations of stepwise twisted structures without geometry optimization. The largest energy difference calculated was 0.3 kJ/mol (between 10° and 70° dihedral angles). Contrary to the expectation and in contrast to tolane, enhancement of the rotational barrier due to hydroxy substitution was not detectable with the diyne-containing model compound. However, because of the minuteness of the barriers for both diyne-containing model compounds, we should not draw any conclusions other than that both barriers are well below kT at ordinary temperature. From a comparison of the calculated rotational barriers, we ought to expect a somewhat smaller conjugation

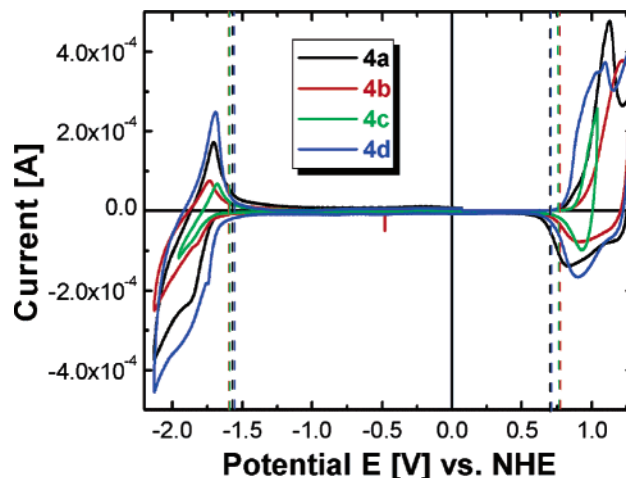


Figure 5. CV curves of polymers 4a–d. The vertical lines show the redox onset values as obtained by EVS.

length for the diyne-linked polymers at ordinary temperature in comparison to the yne-linked polymers. The optical and photophysical properties are determined by a very subtle interplay between electronic interactions within the polymer backbone including donating effects of substituents, steric restrictions due to the side chains and packing effects, and π – π interactions in the condensed state.

Electrochemical Properties. Electrochemical investigations were carried out through the combination of cyclic voltammetry (CV) and electrochemical voltage spectroscopy (EVS), enabling a more exact determination of the HOMO and LUMO levels and the concomitant electrochemical energy gap, E_{g}^{ec} .^{25–27}

Figure 5 shows the CV curves of polymers 4a–d recorded at 10 mV/s scan speed; the lines indicate the onset potentials for the polymers according to the color code. All polymers show reversible redox behavior but are not stable upon many cycles. Comparison of the electrochemical data of polymers 4a–d together with MDMO-PPV²⁵ is presented in Table 4.

The insertion of the second yne unit in 4a–d leads to an increase of the oxidation and reduction onset potentials and consequently to an enhancement of their electron affinity compared to the corresponding yne-containing polymers 6a–d and MDMO-PPV. Their HOMO and LUMO levels are comparatively lowered as can be noticed in the Figure 6, where the energy level diagram of the compounds is presented. The insulating (i.e., shielding) effects of bulky 2-ethylhexyl or longer octadecyl side chains, accounting for considerable discrepancy ΔE_{g} between optical and electrochemical band-gap energies in polymers 6,^{16,28–30} are minimal in polymers 4 due to the “wider opening” caused by the introduction of the second yne unit, which not only

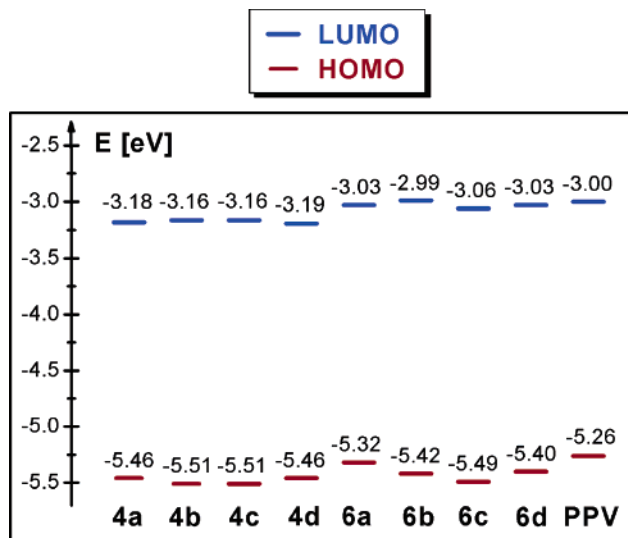


Figure 6. Position of the HOMO and LUMO of the polymers **4a–d**, **6a–d**, and MDMO-PPV in the Fermi energy scale.

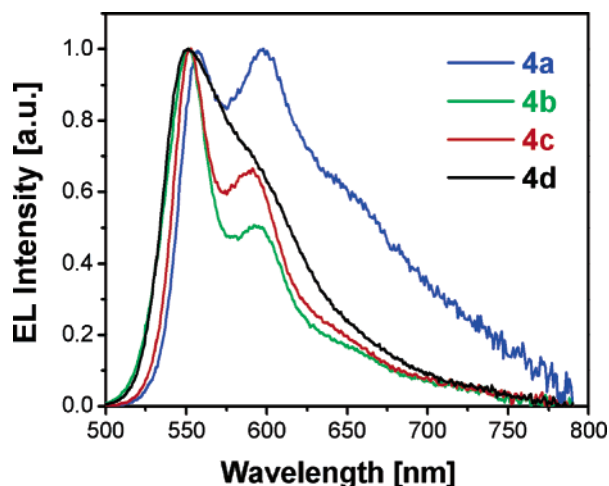


Figure 7. Electroluminescence spectra measured at 5 V of devices of configuration ITO/PEDOT:PSS/polymer **4**/Ca/Al.

Table 5. LED Parameters from Devices of Configuration ITO/PEDOT:PSS/Polymer **4**/Ca/Al

code	λ_{EL} [nm]	luminance at 100 A/cm ⁻² [cd/m ⁻²]	max efficiency [cd/A]	turn-on voltage [V]
4a	557	340	0.32	2.8
4b	552	400	0.42	3
4c	552	1200	1.25	2
4d	552	506	0.54	2.4

facilitates the diffusion of the counterion ClO₄⁻ from the bulk electrolyte to the oxidation site to balance the charges during the oxidation process but also enables an easy transport of charges from the polymer to the electrode (or vice versa).

Electroluminescent Properties. LED devices of configuration ITO/PEDOT:PSS/polymer **4**/Ca/Al, designed with polymers **4a–d**, emit green light at 552 nm for **4b–d** and at 557 nm for **4a**. The EL spectra, depicted in Figure 7, are similar in shape and maxima to the solid-state PL spectra, suggesting emission from the same excited states in both radiative processes. The current–voltage and luminance–voltage characteristics of the devices are shown in Supporting Information Figure S5. Table 5 summarizes the EL parameters of the devices. All devices show low turn-on voltages between 2 and 3 V due to enhanced electron affinity;

best EL parameters, however, resulted from the device made from the 2-ethylhexyl-substituted polymer **4c**.

Conclusions

Four diyne-containing poly(*p*-phenylene–vinylene) derivatives, **4a–d**, have been synthesized, and their chemical structure as well as solid-state properties have been thoroughly characterized. The disparity of the degree of polymerization, *n* (4 for **4b** and **4d**, 8 for **4a**, and 22 for **4c**), might be explained with the side-chain-dependent differences in reactivity of the different reactive species during the polycondensation process. *n*-dependent absorption and emission spectra in dilute chloroform solution as well as *n*-dependent thin film absorption spectra were observed. Following conclusions can be drawn from the comparison of the properties of polymers **4a–b** and their yne-containing counterparts **6a–d**: (1) Despite the difference in their conjugation pattern, both types of compounds show identical photophysical properties as confirmed from fluorescence kinetics measurements and theoretical calculations. (2) The introduction of a second yne unit in **4** lowers their HOMO and LUMO levels relative to **6** due to enhanced electron affinity. (3) The “wider opening” in the backbone of **4** caused by the diyne unit facilitates the migration of charges during the *n*- and *p*-doping processes leading to smaller values of ΔE_g , when bulky 2-ethylhexyloxy or longer octadecyloxy are grafted on phenylene–vinylene segment of the polymers. This is in contrast to polymers **6**, where the insulating effects of bulky or longer side chains led to remarkable ΔE_g values. LED devices of configuration ITO/PEDOT:PSS/polymer **4**/Ca/Al exhibited low turn-on voltage between 2 and 3 V due to enhanced electron affinity.

Supporting Information Available: Experimental description, synthesis and characterization of the material, ¹³C NMR spectrum of polymer **4c**, POM morphological observation for melt-crystallized thin film of polymer **4b**, powder X-ray diffraction intensity distributions of polymers **4a–d**, calculated S₁–S₀ difference densities for unsubstituted oligomers of **4** and **6**, and current density–voltage and luminance–voltage characteristics of LED devices from polymers **4**. This material is available free of charge via the Internet at <http://pubs.acs.org>.

References and Notes

- (1) Hadziioannou, G.; van Hutten, P. F., Eds.; *Semiconducting Polymers: Chemistry, Physics and Engineering*, 1st ed.; Wiley-VCH: Weinheim, Germany, 2000.
- (2) Burroughes, J. H.; Bradley, D. D. C.; Brown, A. R.; Marks, R. N.; MacKays, K.; Friend, R. H.; Burn, P. L.; Holmes, A. B. *Nature (London)* **1990**, *347*, 539.
- (3) Kraft, A.; Grimsdale, A. C.; Holmes, A. B. *Angew. Chem.* **1998**, *110*, 416.
- (4) Yang, X. Y.; Neher, D.; Hertel, D.; Däubler, T. T. *Adv. Mater.* **2004**, *16*, 161.
- (5) Horowitz, G. *Adv. Mater.* **1998**, *10*, 365.
- (6) Würtner, F. *Angew. Chem.* **2001**, *40*, 1037.
- (7) Krebs, F. C.; Jørgensen, M. *Macromolecules* **2003**, *36*, 4374.
- (8) Brabec, C. J.; Sariciftci, N. S.; Hummelen, J. C. *Adv. Funct. Mater.* **2001**, *11*, 15.
- (9) (a) Winder, C.; Sariciftci, N. S. *J. Mater. Chem.* **2004**, *14*, 1077. (b) Hoppe, H.; Sariciftci, N. S. *J. Mater. Res.* **2004**, *19*, 1924.
- (10) Gebeheyu, D.; Pfeifer, M.; Maennig, B.; Drechsel, J.; Werner, A.; Leo, K. *Thin Solid Films* **2004**, *29*, 451.
- (11) Sariciftci, N. S.; Smilowitz, L.; Heeger, A. J.; Wudl, F. *Science* **1992**, *258*, 1474.
- (12) Yamamoto, T.; Yamada, W.; Takagi, M.; Kizu, K.; Maruyama, T.; Tsukasa, O. N.; Tomaru, S.; Kurihara, T.; Kaino, T.; Kubota, K. *Macromolecules* **1994**, *27*, 6620.
- (13) (a) Hernandez, S.; Ogawa, T. *Polym. Bull. (Berlin)* **2001**, *47*, 127. (b) Miura, H.; Ogawa, T. *Polym. Bull. (Berlin)* **2002**, *49*, 103. (c) Ogawa, T. *Prog. Polym. Sci.* **1995**, *20*, 943.

- (14) (a) Bosshard, C.; Spreiter, R.; Günter, P.; Tykwinski, R. R.; Schreiber, M.; Diederich, F. *Adv. Mater.* **1996**, *8*, 231. (b) Gubler, U.; Bosshard, C.; Günter, P.; Balakina, M. Y.; Cornil, J.; Bredas, J. L.; Martin, R. E.; Diederich, F. *Opt. Lett.* **1999**, *24*, 1599. (c) Gubler, U.; Bosshard, C. *Phys. Rev. B.* **2000**, *61*, 10702.
- (15) Kuzyk, M. G. *Opt. Lett.* **2000**, *25*, 1183.
- (16) Egbe, D. A. M.; Carbonnier, B.; Ding, L.; Mühlbacher, D.; Birckner, E.; Pakula, T.; Karasz, F. E.; Grummt, U.-W. *Macromolecules* **2004**, *37*, 7451.
- (17) Egbe, D. A. M.; Roll, C. P.; Birckner, E.; Grummt, U.-W.; Stockmann, R.; Klemm, E. *Macromolecules* **2002**, *35*, 3825. (b) Egbe, D. A. M.; Roll, C. P.; Klemm, E. *Des. Monomers Polym.* **2002**, *5*, 245. (c) Egbe, D. A. M.; Birckner, E.; Klemm, E. *J. Polym. Sci., Part A: Polym. Chem.* **2002**, *40*, 2670. (d) Wilson, J. N.; Windscheif, P. M.; Evans, U.; Myrick, M. L.; Bunz, U. H. F. *Macromolecules* **2002**, *35*, 8681.
- (18) Chu, Q.; Pang, Y.; Ding, L.; Karasz, F. E. *Macromolecules* **2003**, *36*, 3848. (b) Egbe, D. A. M.; Bader, C.; Nowotny, J.; Günther, W.; Klemm, E. *Macromolecules* **2003**, *36*, 5459. (c) Egbe, D. A. M.; Bader, C.; Klemm, E.; Ding, L.; Karasz, F. E.; Grummt, U.-W.; Birckner, E. *Macromolecules* **2003**, *36*, 9303. (d) Zhokhavets, U.; Goldhahn, R.; Gobsch, G.; Al-Ibrahim, M.; Roth, H.-K.; Sensfuss, S.; Klemm, E.; Egbe, D. A. M. *Thin Solid Films* **2003**, *444*, 215.
- (19) (a) Egbe, D. A. M.; Stockmann, R.; Hotzel, M. *J. Opt. A: Pure Appl. Opt.* **2004**, *6*, 791. (b) Egbe, D. A. M.; Bader, C.; Nowotny, J.; Klemm, E. *Proc. SPIE* **2004**, *5215*, 79. (c) Ding, L.; Egbe, D. A. M.; Karasz, F. E. *Macromolecules* **2004**, *37*, 6124. (d) Egbe, D. A. M.; Sell, S.; Ulbricht, C.; Birckner, E.; Grummt, U.-W. *Macromol. Chem. Phys.* **2004**, *205*, 2105.
- (20) Lu, S.-L.; Yang, M.-J.; Bai, F.-L. *Macromol. Rapid Commun.* **2004**, *25*, 968.
- (21) Bunz, U. H. F. *Chem. Rev.* **2000**, *100*, 1605 and references therein.
- (22) Wagner, M.; Nuyken, O. *Macromolecules* **2003**, *36*, 6716.
- (23) Gaussian 03, Revision B. 04: M. J. Frisch, G. W. Trucks, H. B. Schlegel, G. E. Scuseria, M. A. Robb, J. R. Cheeseman, J. A. Montgomery, Jr., T. Vreven, K. N. Kudin, J. C. Burant, J. M. Millam, S. S. Iyengar, J. Tomasi, V. Barone, B. Mennucci, M. Cossi, G. Scalmani, N. Rega, G. A. Petersson, H. Nakatsuji, M. Hada, M. Ehara, K. Toyota, R. Fukuda, J. Hasegawa, M. Ishida, T. Nakajima, Y. Honda, O. Kitao, H. Nakai, M. Klene, X. Li, J. E. Knox, H. P. Hratchian, J. B. Cross, C. Adamo, J. Jaramillo, R. Gomperts, R. E. Stratmann, O. Yazyev, A. J. Austin, R. Cammi, C. Pomelli, J. W. Ochterski, P. Y. Ayala, K. Morokuma, G. A. Voth, P. Salvador, J. J. Dannenberg, V. G. Zakrzewski, S. Dapprich, A. D. Daniels, M. C. Strain, O. Farkas, D. K. Malick, A. D. Rabuck, K. Raghavachari, J. B. Foresman, J. V. Ortiz, Q. Cui, A. G. Baboul, S. Clifford, J. Cioslowski, B. B. Stefanov, G. Liu, A. Liashenko, P. Piskorz, I. Komaromi, R. L. Martin, D. J. Fox, T. Keith, M. A. Al-Laham, C. Y. Peng, A. Nanayakkara, M. Challacombe, P. M. W. Gill, B. Johnson, W. Chen, M. W. Wong, C. Gonzalez, and J. A. Pople, Gaussian, Inc., Pittsburgh, PA, 2003.
- (24) Göller, A.; Klemm, E.; Egbe, D. A. M. *Int. J. Quantum Chem.* **2001**, *84*, 86.
- (25) Mühlbacher, D. Diploma thesis on "Comparative Study of the Electrochemical and Optical Band Gap of Organic Semiconductors", Johannes Kepler University Linz, Austria, 2002.
- (26) Gomer, R. J.; Tryson, G. *J. Chem. Phys.* **1977**, *66*, 4413.
- (27) Kötz, R.; Neff, H.; Müller, K. *J. Electroanal. Chem.* **1986**, *215*, 331.
- (28) Egbe, D. A. M.; Kietzke, T.; Carbonnier, B.; Mühlbacher, D.; Hörhold, H.-H.; Neher, D.; Pakula, T. *Macromolecules* **2004**, *37*, 8863.
- (29) Chen, Z.-K.; Huang, W.; Wang, L.-H.; Kang, E.-T.; Chen, B. J.; Lee, C. S.; Lee, S. T. *Macromolecules* **2000**, *33*, 9015.
- (30) Yamamoto, T.; Lee, B.-L. *Macromolecules* **2002**, *35*, 2993.

MA0507490